AIP | The Journal of Chemical Physics

Emerging activity in bilayered dispersions with wake-mediated interactions

Jörg Bartnick, Andreas Kaiser, Hartmut Löwen, and Alexei V. Ivlev

Citation: The Journal of Chemical Physics **144**, 224901 (2016); doi: 10.1063/1.4953225
View online: http://dx.doi.org/10.1063/1.4953225
View Table of Contents: http://scitation.aip.org/content/aip/journal/jcp/144/22?ver=pdfcov
Published by the AIP Publishing

Emerging activity in bilayered dispersions with wake-mediated interactions

Jörg Bartnick,[1,a)] Andreas Kaiser,[2] Hartmut Löwen,[1] and Alexei V. Ivlev[3]
[1]*Institut für Theoretische Physik II: Weiche Materie, Heinrich-Heine-Universität Düsseldorf, D-40225 Düsseldorf, Germany*
[2]*Materials Science Division, Argonne National Laboratory, Argonne, Illinois 60439, USA*
[3]*Max-Planck-Institut für Extraterrestrische Physik, D-85741 Garching, Germany*

(Received 5 April 2016; accepted 19 May 2016; published online 8 June 2016)

In a bilayered system of particles with wake-mediated interactions, the action-reaction symmetry for the effective forces between particles of different layers is broken. Under quite general conditions we show that, if the interaction nonreciprocity exceeds a certain threshold, this creates an active dispersion of self-propelled clusters of Brownian particles. The emerging activity promotes unusual melting scenarios and an enormous diffusivity in the dense fluid. Our results are obtained by computer simulation and analytical theory and can be verified in experiments with colloidal dispersions and complex plasmas. *Published by AIP Publishing.* [http://dx.doi.org/10.1063/1.4953225]

I. INTRODUCTION

Effective forces between mesoscopic particles often become nonreciprocal when the interactions are mediated by a nonequilibrium environment. Such situations can be realized in various soft matter systems — most notably in colloidal dispersions[1–6] and complex plasmas,[7–10] where microparticles are embedded, respectively, in a liquid solvent or a dilute weakly ionized gas. In particular, the action-reaction symmetry in these systems is broken when the surrounding fluid moves with respect to the particles,[11–15] or when the interaction of molecules with the particle surface is out of equilibrium.[1,2,5,6]

Studies of nonreciprocal interactions have gained increased interest in recent time. When the dynamics of individual particles is undamped (Newtonian) or weakly damped (i.e., when the relevant dynamical timescales are much shorter than the damping time),[12] which is typical for complex plasmas, one can observe a remarkable state of *detailed dynamic equilibrium* with different species having different temperatures. For Brownian dynamics, it has recently been shown that mixtures of diffusiophoretic colloids experience effective nonreciprocal forces which stimulate the formation of stable aggregates (so-called active molecules)[6] and trigger collective oscillatory motion.[16]

In this paper, we consider a broad generic class of nonreciprocal interparticle forces, the so-called wake-mediated interactions. Particles embedded in a flowing medium generate wakes, which contribute to the interactions with neighbors in a nonreciprocal way.[9–11] Similarly, particles emitting chemicals in a certain direction generate asymmetric concentration fields — artificial "chemical wakes," also exerting non-reciprocal forces on the neighbors.[16,17] In both cases, the action-reaction symmetry is only restored for identical particles, forming a perfect monolayer perpendicular to the direction of wakes. Therefore, here we consider a quasi two-dimensional system of Brownian particles[18] which are kept into stable bilayers by external fields such as electric, magnetic, gravitational, or optical fields. Under quite general conditions posed on the mutual reciprocal and nonreciprocal forces, we observe a continuous transition from inactive (stacked) pairs to active units, indicating the emergence of active fluids. Different from ordinary active particle systems,[17,19,20] these active units can break and become passive again. Using analytical theory and simulation including hydrodynamic interactions between the particles, we explore the full density regime up to freezing and find an unusual melting upon densification, along with a reentrant freezing and an enormous diffusivity in the concentrated fluid.

The paper is organized as follows: In Sec. II we specify our model, perform a stability analysis for small clusters in Sec. III, and describe our simulation in Sec. IV. Results are discussed in Sec. V and summarized in Sec. VI.

II. MODEL

The motion of a particle i at position $\mathbf{r}_i$ in the plane is governed by the fully damped Langevin equation[21]

$$\dot{\mathbf{r}}_i = \sum_j \mathbf{L}_{ij} \cdot \left(\mathbf{F}_j + \boldsymbol{\xi}_j\right) + \frac{1}{2} k_B T \sum_j \frac{\partial \mathbf{L}_{ij}}{\partial \mathbf{r}_j}, \qquad (1)$$

where $\mathbf{L}_{ij}$ is the mobility matrix and $\boldsymbol{\xi}_i$ is a random force. The total force $\mathbf{F}_i$ on particle i is given by $\mathbf{F}_i = \sum_j \mathbf{F}_{ji}$, where $\mathbf{F}_{ji}$ is the pair-interaction force exerted by a particle j on the particle i. The random force $\boldsymbol{\xi}_i$ is Gaussian distributed with zero mean, $\langle \boldsymbol{\xi}_i(t) \rangle = 0$, and variance $\langle \boldsymbol{\xi}_i(t) \boldsymbol{\xi}_j(t') \rangle = 2\, \mathbf{L}_{ij}^{-1}\, k_B T \delta(t - t')$, where T is the thermostat temperature, k_B the Boltzmann constant, $\delta(t)$ the Dirac delta function, and $\mathbf{L}^{-1}$ the inverse of $\mathbf{L}$. In this paper, we include hydrodynamic interactions in the zero-temperature limit and neglect them at finite temperatures. The latter approach is justified when the suspension is highly dilute but still strongly interacting. Then, each mobility matrix reduces to $\mathbf{L}_{ij} = \gamma_i^{-1} \delta_{ij} \mathbf{I}$, with the unit matrix $\mathbf{I}$ and a friction coefficient γ_i. In the zero-temperature limit, we consider the mobility matrix to be approximated by the Oseen tensor[21]

a)Electronic mail: bartnick@thphy.uni-duesseldorf.de

$$\mathbf{L}_O(\mathbf{r}) = \frac{3R_H}{4\gamma_i r}(\mathbf{I} + \hat{\mathbf{r}}\hat{\mathbf{r}}), \tag{2}$$

where R_H is the hydrodynamic radius, $r = |\mathbf{r}|$ and $\hat{\mathbf{r}} = \mathbf{r}/r$. Thus, we have $\mathbf{L}_{ij} \approx \mathbf{L}_O(\mathbf{r}_i - \mathbf{r}_j)$ for $i \neq j$ and $\mathbf{L}_{ii} = \mathbf{I}/\gamma_i$.

We consider a typical situation when interactions between particles are isotropic in the plane. In this case the mutual forces between particles i and j are radial, i.e., $\mathbf{F}_{ij} = F_{ij}\mathbf{n}_{ij}$ with $\mathbf{n}_{ij}$ being the unit vector from i to j, and F_{ij} only depends on the absolute distance $r_{ij} = |\mathbf{r}_i - \mathbf{r}_j|$. Furthermore, we introduce species A and B and attribute particles to the same species if their pair interactions are reciprocal, i.e., $F_{\mathrm{AA}}(r) = F_{\mathrm{BB}}(r) = -d\varphi_{\mathrm{r}}(r)/dr$. A generic form for the forces between different species,

$$F_{\mathrm{AB,BA}}(r) = -d\varphi_{\mathrm{r}}(r)/dr \pm d\varphi_{\mathrm{n}}(r)/dr, \tag{3}$$

is a superposition of the reciprocal (r) and nonreciprocal (n) components, determined by the respective potentials $\varphi_{\mathrm{r,n}}$. The latter are related to the potential φ_{ij} generated by the particle i at the location of the particle j via $\varphi_{\mathrm{r,n}} = \frac{1}{2}(\varphi_{ji} \pm \varphi_{ij})$. Thus, the pair interactions are reciprocal if $\varphi_{ij} = \varphi_{ji}$ and are nonreciprocal otherwise.

An important class of a constant nonreciprocity is realized when $\varphi_{\mathrm{r}}(r)$ and $\varphi_{\mathrm{n}}(r)$ are similar functions, i.e., when the nonreciprocity $\varphi_{\mathrm{n}}(r)/\varphi_{\mathrm{r}}(r) \equiv \Delta = \mathrm{const}$. For the undamped (Newtonian) or weakly damped dynamics with $\Delta = \mathrm{const}$, the equations of motion can be equivalently transformed into a reciprocal form by a simultaneous proper renormalization of the interaction forces and masses, i.e., such dynamics can in fact always be described by a (pseudo) Hamiltonian.[12] It is noteworthy that for the Brownian dynamics with nonreciprocal interactions one can employ a similar approach. By renormalizing the interactions with Eq. (3) of Ref. 12, and introducing the renormalized damping coefficients $\tilde{\gamma}_{\mathrm{A,B}} = \gamma_{\mathrm{A,B}}/(1 \mp \Delta)$, we readily transform Eq. (1) to the form where the interactions are reciprocal, while the solvent temperatures for different species A and B are different and equal to $\widetilde{T}_{\mathrm{A,B}} = T/(1 \mp \Delta)$. Interestingly, such a "hetero-Brownian" model has been recently introduced in a different context, to describe DNA dynamics,[22,23] and was also proposed for colloidal pairs under external forcing.[24–26]

In our model, we adopt a binary mixture of point-like particles whose direct (electrostatic) interactions are characterized by the charges Q_{A} and Q_{B}. The particles are confined in a horizontal xy-plane in two layers with a height difference h, as sketched in Fig. 1. The point-like approximation is justified as long as the distance between the particles is much larger than their diameter. For non-reciprocal particle-wake forces we have two representative realizations in mind, both leading to effective Yukawa interactions: The first one can be obtained with catalytically active Janus colloids,[27,28] where each particle emits a chemical from the lower segment of the surface, thus generating "chemical" wakes (the vertical orientation of such particles can be stabilized in an external magnetic field[29]). The emitted chemicals decompose with a constant rate,[30] such that the effective interaction between the chemical wake and a neighboring particle is of Yukawa form. The second realization is an externally imposed micro-ion flow, parallel to the vertical

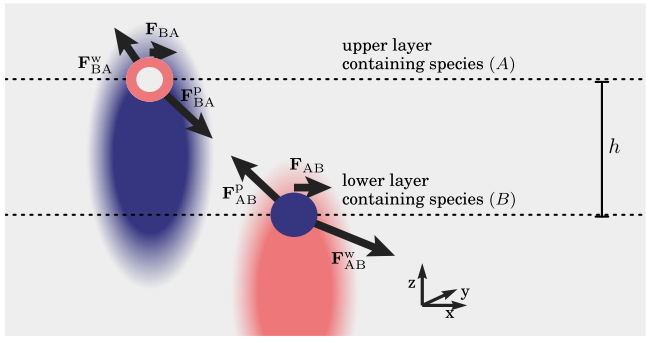

FIG. 1. Schematic sketch of nonreciprocal wake-mediated interactions. The particle species A and B are confined in the upper and lower layers, respectively. While the direct interparticle forces are reciprocal, $\mathbf{F}^{\mathrm{p}}_{\mathrm{BA}} + \mathbf{F}^{\mathrm{p}}_{\mathrm{AB}} = \mathbf{0}$, the particle-wake forces are nonreciprocal, $\mathbf{F}^{\mathrm{w}}_{\mathrm{BA}} + \mathbf{F}^{\mathrm{w}}_{\mathrm{AB}} \neq \mathbf{0}$ such that for the total forces $\mathbf{F}_{\mathrm{AB}} \neq -\mathbf{F}_{\mathrm{BA}}$.

z-axis, which induces an "electrostatic" wake below each particle, while the fluid remains at rest. In both cases, the wake is mimicked by a point-like effective "charge" q_i at the distance δ below each particle.

The total interaction force is a combination of the direct particle interaction and the particle-wake interaction. The force depends on several free parameters whose combination determines emergence of different self-organization phenomena. In this letter we chose a certain set of parameters, demonstrating variety of the emerging activity, and identify a general necessary condition for the activity onset [see Eq. (5) below]. Let us introduce the three-dimensional particle coordinates $\mathbf{R}_i$ and the corresponding coordinates $\mathbf{r}_i$ in the horizontal plane. Then the force $\mathbf{F}_{ij} = -\partial\varphi_{ij}/\partial\mathbf{r}_j$ exerted in the horizontal plane by the particle i on the particle j is determined by the potential $\varphi_{ij} = Q_iQ_jY(R_{ij}) + q_iQ_jY(R^{\mathrm{w}}_{ij})$, where $Y(R) = R^{-1}e^{-R/\lambda}$ is the (unity charge) Yukawa potential which depends on the distance $R_{ij} = |\mathbf{R}_i - \mathbf{R}_j|$ between the particles as well as on the distance $R^{\mathrm{w}}_{ij} = |\mathbf{R}_i - \mathbf{R}_j - \delta\mathbf{n}_z|$ between the particle j and the wake center of the particle i;[32,33] here, we assume that a Yukawa potential for both forces has the same effective screening length λ and that $q_i \propto -Q_i$.[31,42,43] For particles in the same layer, A or B, we have $R^{\mathrm{w}}_{ij} = R^{\mathrm{w}}_{ji}$; therefore, $\varphi_{\mathrm{n}} = 0$ (since $q_iQ_j = q_jQ_i$), and hence the forces are reciprocal. For the AB interactions the symmetry is broken, $R^{\mathrm{w}}_{ij} \neq R^{\mathrm{w}}_{ji}$, and the forces are nonreciprocal. For simplicity, particles A and B have charges of the same magnitude and opposite signs, $Q_{\mathrm{A}} = -Q_{\mathrm{B}} \equiv Q$, the same friction coefficients, $\gamma_{\mathrm{A}} = \gamma_{\mathrm{B}} \equiv \gamma$, and the height difference is $h = \lambda$. A natural measure of nonreciprocity in this case is the relative wake charge, $\tilde{q} = -q_i/Q_i > 0$.

III. STABILITY ANALYSIS FOR SMALL CLUSTERS

In order to illustrate a tendency of particles with nonreciprocal interactions to self-organize themselves with increasing $\tilde{q}$ and to identify the characteristic building blocks of this complex process, let us consider the formation of small clusters in the absence of hydrodynamic interactions. Then, the equilibrium configurations for a cluster of N particles are determined from the force balance in the *horizontal* plane,

$$\sum_{j}^{N} \mathbf{F}_{ji}(r_{ij}) = \mathbf{F}, \tag{4}$$

where the net force $\mathbf{F}$ is a constant horizontal vector for $\forall i \in [1, N]$. We apply the standard stability analysis of the derived configurations in the zero-temperature limit. This corresponds to the eigenvalue problem $\det\left(\partial \mathbf{F}_{ij}/\partial \mathbf{r}_j|_{\mathrm{eq}} - \gamma\omega \mathbf{I}\right) = 0$, where $\ldots|_{\mathrm{eq}}$ denotes the $(2N \times 2N)$ dynamical matrix calculated for the equilibrium configurations.

A. Doublets

A pair of particles of different species form an equilibrium *doublet* with the horizontal separation r_D when $F_{\mathrm{AB}}(r_D) = -F_{\mathrm{BA}}(r_D) \equiv F$; the doublet is stable if $d\left[F_{\mathrm{AB}}(r) + F_{\mathrm{BA}}(r)\right]/dr|_{r=r_D} < 0$. From Eq. (3) we conclude that the stability condition is only fulfilled when the reciprocal component of the force is equal to zero, $d\varphi_{\mathrm{r}}(r)/dr|_{r=r_D} = 0$.

For a vertical pair $r_D = 0$ – we call it *an inactive doublet* – two regimes can be distinguished: (i) When $dF_{ij}(r)/dr\big|_{r=0} < 0$ for both particles, they return to the equilibrium after a small perturbation. Below we demonstrate that this case, sketched in Fig. 2(a), is observed for a "weak" nonreciprocity, when the relative wake charge is smaller than a certain critical value, $\tilde{q} < \tilde{q}_{\mathrm{cr1}}$ (i.e., this always occurs for reciprocal interactions). (ii) When $dF_{ij}(r)/dr\big|_{r=0} > 0$ for one of the particles, the restoring forces are pointed in the same direction, as shown in Fig. 2(b). The equilibrium in this case, corresponding to $\tilde{q}_{\mathrm{cr1}} < \tilde{q} < \tilde{q}_{\mathrm{cr2}}$, would only be restored in the zero-temperature limit; in the presence of an infinitesimal thermal noise the doublet should break apart.

Under the general condition

$$d\varphi_{\mathrm{r}}(r)/dr|_{r=r_D} = 0 \ \text{ and } \ d\varphi_{\mathrm{n}}(r)/dr|_{r=r_D} \neq 0, \tag{5}$$

satisfied for $r_D > 0$, a pair emerges which is self-propelled in the direction $\mathbf{n}_{\mathrm{AB}}$ with the velocity $v_D = -\gamma^{-1} d\varphi_{\mathrm{n}}(r)/dr|_{r=r_D}$. Such clusters will be referred to as *active doublets* and occur when $\tilde{q} > \tilde{q}_{\mathrm{cr2}}$. Note that for a constant nonreciprocity, Δ = const, stable doublets are always at rest, since $\varphi_{\mathrm{n}}(r) = \Delta\varphi_{\mathrm{r}}(r)$ and therefore the nonreciprocal force is equal to zero at $r = r_D$.[34] Equation (5) represents the necessary condition for the emerging activity, which can be satisfied for various combinations of the interaction parameters (e.g., when Q_{A} and Q_{B} have the same sign, but the direct and the particle-wake interactions are characterized by different screening lengths).

Figures 2(d) and 2(e) illustrate the results of the stability analysis in the horizontal plane, performed in the zero-temperature limit. In the present example, two particles of different species are stacked on top of each other (i.e., they form an inactive doublet) when the relative wake charge is smaller than $\tilde{q}_{\mathrm{cr2}} \simeq 0.74$. For larger $\tilde{q}$, the separation r_D continuously increases and an active doublet moves along its symmetry axis, with the velocity v_D which varies non-monotonically with $\tilde{q}$. Thus, in dilute systems (with infinitesimal number density) one can expect the formation of multiple individual doublets. Hydrodynamic interactions do not influence the pair separation r_D but cause a velocity increase. Interestingly, the leading term for the hydrodynamic

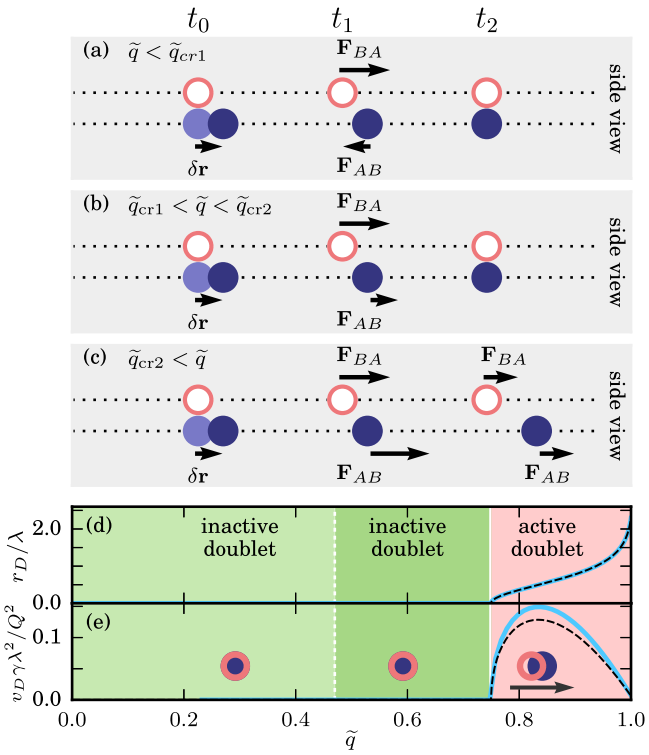

FIG. 2. Stable configurations of two-particle clusters, depending on the relative wake charge $\tilde{q}$. ((a)-(c)) Sketches illustrate three distinct regimes (side view): For $\tilde{q} < \tilde{q}_{\mathrm{cr1}}$, particles form a stable vertical pair, *an inactive doublet*, since the restoring forces $\mathbf{F}_{\mathrm{AB}}$ and $\mathbf{F}_{\mathrm{BA}}$ exerted by a small perturbation pull the particles back; for $\tilde{q}_{\mathrm{cr1}} < \tilde{q} < \tilde{q}_{\mathrm{cr2}}$, the vertical pair remains stable only in the zero-temperature limit assumed here, since $\mathbf{F}_{\mathrm{AB}}$ and $\mathbf{F}_{\mathrm{BA}}$ are pointed in the same direction; for $\tilde{q} > \tilde{q}_{\mathrm{cr2}}$, the particles form *an active doublet* with a finite horizontal separation, moving along the force $\mathbf{F}_{\mathrm{AB}} = \mathbf{F}_{\mathrm{BA}}$. (d) and (e) Equilibrium horizontal separation of the doublet, r_D (normalized by λ) and the corresponding doublet velocity v_D (normalized by $Q^2/\lambda^2\gamma$), the shading indicates the stability regimes illustrated in (a)-(c). The results are for the wake length $\delta = 0.2\lambda$, $h = \lambda$, and $R_H = 0$ (black dashed line), as well as $R_H = 0.2\lambda$ (blue solid line).

far-field for an active doublet is a force monopole, as opposed to a standard microswimmer where it is a force dipole.[20]

For a finite number density ρ (number of particles per unit area) in systems without hydrodynamic interactions, we analyze the stability of crystalline structures in the zero-temperature limit. The time-dependent coordinate of the ith particle is presented as a sum of its equilibrium lattice position and a displacement, $\mathbf{r}_i(t) = \mathbf{r}_{\mathrm{eq},i} + \mathbf{u}_i(t)$. The interaction force, Eq. (3), is then expanded to the first order in $\mathbf{u}_i$ and substituted in Eq. (1). Using $\mathbf{u}_i \propto \exp(i\mathbf{k} \cdot \mathbf{r}_{\mathrm{eq},i} + \omega t)$, the dispersion relations $\omega(\mathbf{k})$ are derived as eigenvalues of the resulting dynamical matrix.[32] We examine a vertically stacked hexagonal lattice and an interdigitated hexagonal lattice, the stability requires $\mathrm{Re}\,\omega(\mathbf{k}) < 0$ for all $\mathbf{k}$ from the first Brillouin zone of the lattice.

Let us now study the effect of hydrodynamic interactions on a doublet, consisting of a particle of species A and one of species B in the dilute limit. The general requirement for stable clusters is the equality of the velocities,

$$\dot{\mathbf{r}}_{\mathrm{A}} = \dot{\mathbf{r}}_{\mathrm{B}}. \tag{6}$$

The equation of motion of the A particle can be written as

$$\dot{\mathbf{r}}_A = \frac{1}{\gamma}\mathbf{F}_A(\mathbf{r}_A - \mathbf{r}_B) + \left[\frac{3R_H}{4\gamma\tilde{r}}\left(1 + \frac{r^2}{\tilde{r}^2}\right)\right]\mathbf{F}_B(\mathbf{r}_B - \mathbf{r}_A), \quad (7)$$

with $\tilde{r} = \sqrt{r^2 + h^2}$; the respective equation for the B particle is obtained by the A ↔ B permutation. Equation (6) is only fulfilled if $F_{AB}(r_D) = -F_{BA}(r_D)$, as in the case without hydrodynamic interactions. Thus, Eq. (5) remain valid also for a finite hydrodynamic radius. Figure 2 shows the result for a doublet with and without hydrodynamic interactions. The doublet distance r_D remains unchanged, while the doublet velocity is slightly increased.

B. Triplets

For three particles, there is a variety of possible *triplet* configurations. To start with, let us consider a cluster composed of one particle B and two particles A with negligible hydrodynamic interactions. We work in the frame of reference of the first (B) particle, i.e., the coordinates of the second and third (A) particles are $\mathbf{r}_{2,3}$. In this case, the general equilibrium condition, Eq. (4), can be identically transformed to the following two equations for the particle coordinates (plus one equation for the net force $\mathbf{F}$):

$$\tilde{F}(r_2)\mathbf{n}_2 + \tilde{F}(r_3)\mathbf{n}_3 = \mathbf{0}, \quad (8a)$$

$$2F_{AA}(r_{23})\mathbf{n}_{32} - F_{BA}(r_3)\mathbf{n}_3 + F_{BA}(r_2)\mathbf{n}_2 = \mathbf{0}, \quad (8b)$$

with $\tilde{F}(r) \equiv F_{BA}(r) + 2F_{AB}(r)$. In the reverse case, where clusters are composed of one A and two B particles, the labels are simply to be swapped.

Using Eq. (8a), one can distinguish two principal cases: (i) $\tilde{F}(r_{2,3}) \neq 0$, then solutions exist only for $\mathbf{r}_2 \parallel \mathbf{r}_3$; (ii) $\tilde{F}(r_2) = \tilde{F}(r_3) = 0$, then solutions are possible for noncollinear $\mathbf{r}_2$ and $\mathbf{r}_3$.

(i) If $\tilde{F}(r)$ is a monotonic function, the only solution is $\mathbf{r}_2 = -\mathbf{r}_3$; from Eq. (8b) we obtain $F_{AA}(2r) = F_{BA}(r)$, which yields $r_2 = r_3 \equiv r$. Due to symmetry, $F = 0$ and hence we call such configurations *inactive linear triplets*. However, if $\tilde{F}(r)$ is a non-monotonic function, also solutions with $r_2 \neq r_3$ are possible — in this case Eqs. (8a) and (8b) are reduced to $\tilde{F}(r_2) = \tilde{F}(r_3)$ and $2F_{AA}(r_2 + r_3) = F_{BA}(r_2) + F_{BA}(r_3)$. Such asymmetric clusters usually imply a non-vanishing net force, $F \neq 0$, which generates a directed propulsion. We call these configurations *active linear triplets*.

(ii) If $F_{BA}(r)$ is monotonic, solutions for $\mathbf{r}_{2,3}$ are limited to triangles with $r_2 = r_3 \equiv r$ and the apex angle θ, obtained from $F(r) = 0$ and $F_{AA}(2r\sin\frac{1}{2}\theta)/\sin\frac{1}{2}\theta = F_{BA}(r)$. Such configurations are called *active triangular triplets*. Finally, if $F_{BA}(r)$ is a non-monotonic function, triangular triplets with $r_2 \neq r_3$ are possible.

As for the doublets, we apply the standard stability analysis of the derived configurations in the zero-temperature limit.

If the number of particles B is twice as high as the number of A particles, the dependence on $\tilde{q}$ remains the same as in Fig. 2. The "excess" particle B simply remains an *inactive singlet* [see Fig. 3(a)]. On the contrary, in the situation with two particles A for one particle B various active and inactive structures emerge, as presented in Fig. 3(b): An inactive

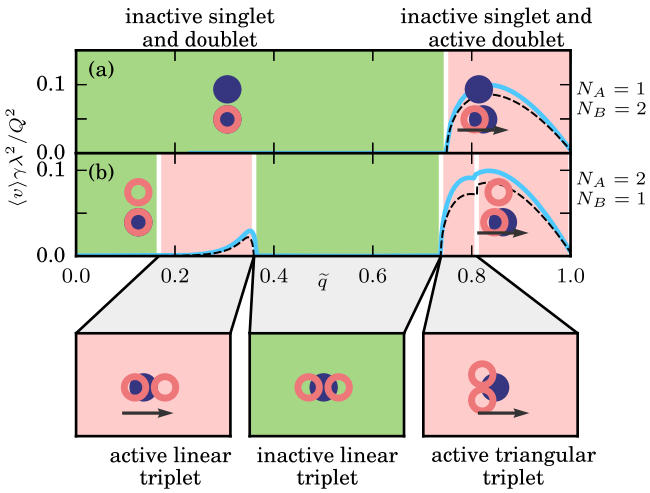

FIG. 3. Stable configurations and velocities of three-particle clusters in the zero-temperature limit. The two possible combinations of the species A and B are shown. The figure legend is the same as in Fig. 2.

doublet and an inactive singlet are formed when $\tilde{q} < 0.17$, while for $\tilde{q} \in (0.17, 0.36)$ they merge into an *active linear triplet*, where the position of particle B is slightly shifted from the center (which determines the propagation direction along the symmetry axis). The linear triplet becomes inactive at $\tilde{q} \in (0.36, 0.74)$. The further increase of the wake charge, $\tilde{q} \in (0.74, 0.81)$, causes particle B to shift perpendicular to the symmetry axis, leading to an *active triangular triplet*. For even larger values of $\tilde{q}$, the triplet breaks apart and an active doublet and an inactive singlet emerge. In a similar manner, one can straightforwardly generalize the analysis for larger clusters or investigate, e.g., the rotation activity.

Figure 4(a) shows the horizontal separation r_1 for the case of $(N_A = 1, N_B = 2)$, where a passive singlet and a doublet form. In the reverse situation $(N_A = 2, N_B = 1)$, we characterize the emerging triplets by their individual bond distances r_2, r_3 [Fig. 4(b)] and the respective apex angle θ

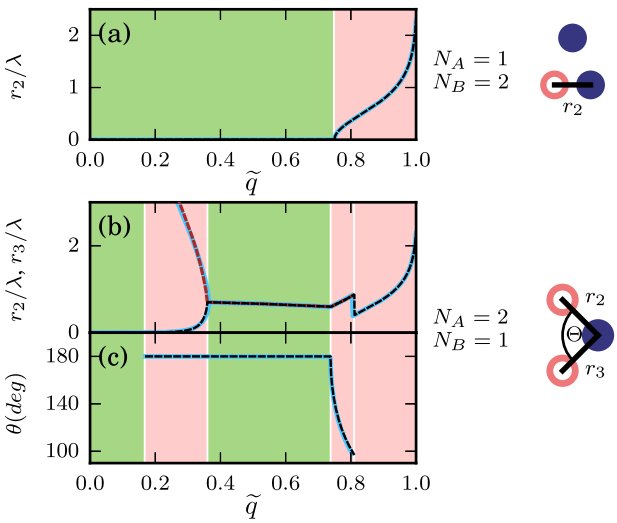

FIG. 4. Equilibrium horizontal separation in the doublet and triplet configurations shown in Fig. 3.

[Fig. 4(c)]. Activity is a result of symmetry breaking, therefore active units are found if $r_2 \neq r_3$ or $\theta < 180°$.

If hydrodynamic interactions are taken into account, the equilibrium condition generalizes towards

$$\dot{\mathbf{r}}_i = \dot{\mathbf{r}} \quad \forall \quad i \in [1, N]\,. \tag{9}$$

Generally, the triplet coordinates derived above do not fulfill this equilibrium condition, which is in contrast with the doublets (where the inclusion of hydrodynamic interactions only induces a rescaling of the velocity). For three particles, we solve Eq. (1) numerically and show the results in Figs. 3 and 4. However, the resulting changes to the particle coordinates are minor, as shown in Fig. 4. Similar to doublets, the inclusion of hydrodynamic interactions merely causes a slight increase of the velocity, see Fig. 3.

IV. COMPUTER SIMULATIONS

We solve the equation of motion, Eq. (1), using a forward time step algorithm in a Brownian dynamics simulation for three distinct cases: when the hydrodynamic interactions are neglected, we consider (i) the zero-temperature limit and (ii) finite temperatures; (iii) the effect of the hydrodynamic interactions is studied in the zero-temperature limit. We use a 2D rectangular simulation box with periodic boundary conditions and the edge ratio $L_y/L_x = \sqrt{3}/2$. The particles are initialized on a distorted stacked hexagonal lattice with a fixed number density $\rho = N/(L_x L_y)$. In the cases (i) and (ii), we use $N = 2 \times 2500$ particles. The respective edge lengths of the simulation domain are varying from $(L_x, L_y) \simeq (240\lambda, 210\lambda)$ at low densities to $(L_x, L_y) \simeq (43\lambda, 38\lambda)$ at $\rho\lambda^2 = 3$. In the case (iii), we use $N = 2 \times 576$ particles, and the simulation domain is between $(L_x, L_y) \simeq (115\lambda, 100\lambda)$ at low densities and $(L_x, L_y) \simeq (28\lambda, 24\lambda)$ at high densities. The modeling of the hydrodynamic interactions is done on the Oseen level with $R_H = 0.2\lambda$, i.e., up to volume fractions of about 15%. For all cases, the wake length is $\delta = 0.2\lambda$, the height between the layers is $h = \lambda$, the time t is measured in units of $\tau = \gamma\lambda^3/Q^2$ and the distance r in units of λ. We set the time step to $\delta t = 0.005\tau$ in the cases (i) and (ii) and to $\delta t = 0.0025\tau$ in case (iii), which ensures proper resolution of the particle dynamics. After initialization, the system is given time of $10^4\tau$ to relax into a steady state. Statistics is gathered for multiple simulations runs with independent initializations and the simulation time of 2500τ. By measuring the displacement of individual particles within the time step, a particle velocity is calculated as $\mathbf{v}_i(t) = [\mathbf{r}_i(t + \delta t) - \mathbf{r}_i(t)]/\delta t$.

V. RESULTS

A. Zero-temperature limit

The above analytical results, see Sec. III, are complemented with a numerical analysis.[36] Figure 5 presents the state diagram of the emerging activity, where we compare the theoretical results against simulations in the zero-temperature limit. The state diagram is plotted in the plane spanned by number density ρ and relative wake charge $\tilde{q}$. We identify

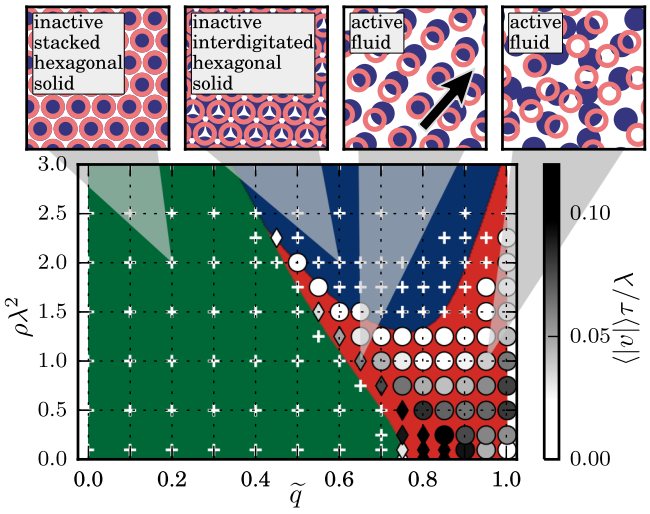

FIG. 5. State diagram in the zero-temperature limit, plotted in the plane of the number density ρ and relative wake charge $\tilde{q}$. Color coding depicts results obtained from the stability analysis, symbols show numerical results. Inactive systems (+) can be either *stacked hexagonal solid* (green background) or *interdigitated hexagonal solid* (blue background). For *active fluid* regimes (○, red background), the average particle velocities are indicated by a gray scale. Diamonds (◊) are used instead of circles if active doublets emerge whose decay time τ_D exceeds a threshold of $10^3\tau$. The states are illustrated by typical snapshots, see also movies in the Supplementary Material.[35]

three distinct domains: Toward the reciprocal limit $\tilde{q} = 0$, the particles form a bilayered *stacked hexagonal crystal* (green); for larger $\tilde{q}$, at increased density the system goes into an *interdigitated hexagonal solid* (blue); for even larger $\tilde{q}$, at low densities we find an *active regime* where the crystal melts (red). In addition, we show the results obtained from the numerical simulations. Here, we differentiate between *inactive solids* (+) and *active fluids* (○). The mobile units of the fluid are active doublets that behave similar to (deformable) active Brownian particles.[37–39] The active regime in the simulations is defined for the average particle velocity $\langle|\mathbf{v}|\rangle$ above a threshold of $10^{-2}\lambda/\tau$. One can see that the emerging state diagram exhibits a reentrant behavior both with ρ and $\tilde{q}$. Notably, for intermediate $\tilde{q}$, there is an anomalous "water-like" melting upon an increase in ρ followed by reentrant freezing. Furthermore, to quantify the stability of doublets we define $N_D(t)$, the average number of particle pairs that remain nearest neighbors over the time interval t. Generally, it is well described by an exponential decay, $N_D(t) \propto e^{-t/\tau_D}$, with a doublet decay time τ_D. Long-living active clusters are marked by a diamond in Fig. 5. The existence of a finite decay time τ_D reveals a qualitative difference of our system to a system of permanently active particles.[17,20,40,41]

We now discuss the characteristics of the *active fluid* in more detail. Let us first introduce the averaged velocity $\langle\mathbf{v}\rangle = \langle[\mathbf{r}_i(t + \delta t) - \mathbf{r}_i(t)]/\delta t\rangle$, see Figs. 6(a) and 6(d), as well as an alignment parameter $c = |\langle\mathbf{v}\rangle| \,/\, \langle|\mathbf{v}|\rangle$, see Figs. 6(b) and 6(e): $c = 1$ for a perfect nematic order and $c = 0$ in a totally disordered case. The stability of doublets is quantified by $N_D(t)$, the averaged number of particle pairs that remain nearest neighbors over the time interval t. The doublet decay time τ_D is shown in Figs. 6(c) and 6(f). If no doublet splits during the simulation time of 2500τ, then τ_D is set to infinity.

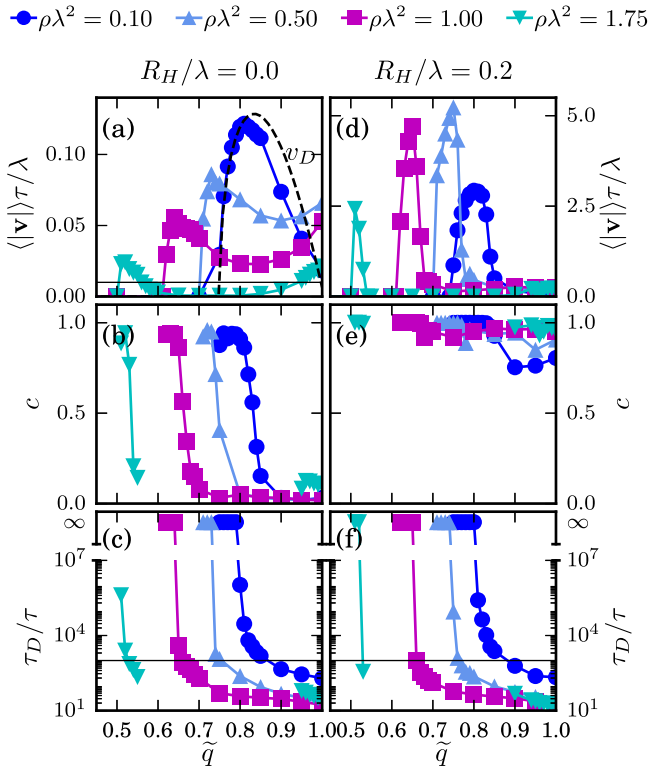

FIG. 6. Characteristics of active fluids: (a) and (d) average particle velocity $\langle|\mathbf{v}|\rangle$, (b) and (e) alignment parameter c, and (c) and (f) decay time of doublets τ_D, plotted versus the relative wake charge $\tilde{q}$ for several values of the number density ρ. The panels on the left show the results for simulations without hydrodynamic interactions, on the right hydrodynamic interactions are included. The dashed line in panel (a) shows the velocity of a single active doublet v_D in the dilute case ($\rho\lambda^2 \ll 1$), the horizontal lines in panels (a), (c) and (f) indicate the threshold values of the velocity ($10^{-2}\lambda/\tau$) and decay time ($10^3\tau$).

Figure 6(a) demonstrates that at low densities ($\rho\lambda^2 = 0.1$), the average velocity $\langle|\mathbf{v}|\rangle$ is well reproduced by the velocity of a single active doublet, v_D, calculated analytically. Above the threshold value of $\tilde{q}_{cr2} = 0.74$, the distance r_D increases, see Fig. 2(d). For this reason, the average velocity first increases with $\tilde{q}$, but then it starts falling off due to decreasing interaction strength of a doublet, see also Fig. 2(e). As the activity sets in, long-living doublets are formed throughout the system and their mutual collisions lead to the velocity alignment, see Fig. 5, since the angle of reflection α_r after their mutual collision is always smaller the incidence angle α_i, as shown in Fig. 7. With increasing the number density ρ the onset of activity shifts towards smaller $\tilde{q}$, whereby the average velocity vs. wake charge becomes a non-monotonic function, leading to a reentrant effect for $\rho\lambda^2 > 1.25$, where an *inactive interdigitated hexagonal solid* emerges, see Fig. 5.

The effects of hydrodynamic interactions are demonstrated in the right panel of Fig. 6. One can see that the effects become significant at higher densities. In comparison with the left panel, we observe a drastic velocity increase, while the alignment remains strong at any $\tilde{q}$. These effects become more pronounced due to the long-range nature of hydrodynamic interactions, so that more particles are involved in the collective motion.

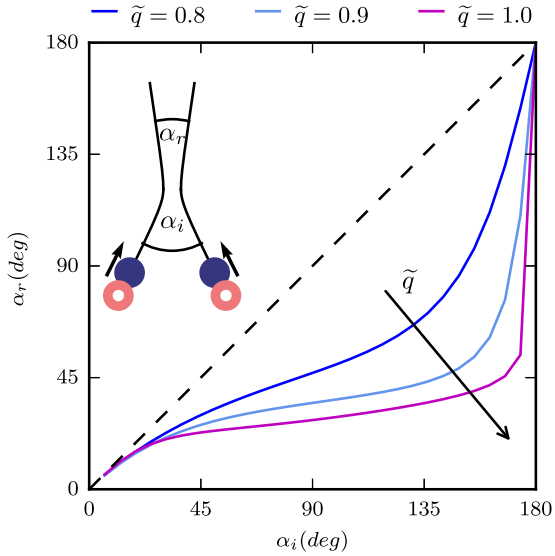

FIG. 7. Angle of reflection α_r versus the incidence angle α_i for a collision of two active doublets, plotted for different values of the relative wake charge $\tilde{q}$. The symmetric scattering, $\alpha_r = \alpha_i$, is indicated by the dashed line.

B. Finite temperature study

Let us study the case of finite temperatures in the absence of hydrodynamic interactions. For a single stacked doublet, where $r_D = 0$, we compute the mean-squared displacement from Eq. (1). We take the Taylor expansion of the forces around the equilibrium positions. Then, the radial force perturbations are $\delta F_{BA}(t) \approx C_A\,[\delta r_A(t) - \delta r_B(t)]$ and $\delta F_{AB}(t) \approx C_B\,[\delta r_B(t) - \delta r_A(t)]$, where C_A and C_B are the prefactors of the linear-order terms in the expansion. We define $\mathbf{A}$ as a matrix containing these prefactors, such that Eq. (1) can be written as

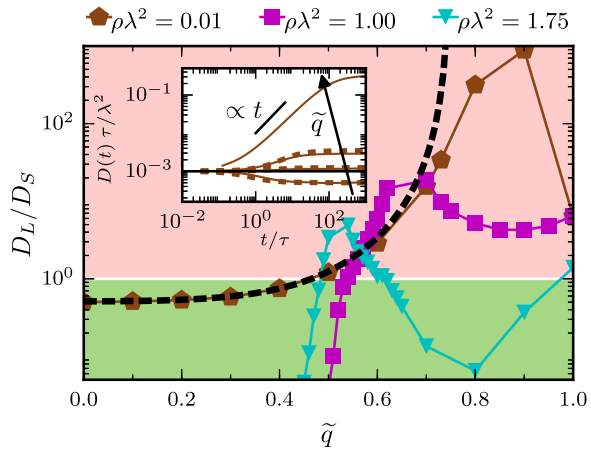

FIG. 8. Ratio of the long-time to short-time diffusion coefficients, D_L/D_S, obtained from the time dependent diffusion coefficient $D(t)$ for a finite temperature $T = 10^{-3}\,Q^2/(k_B\lambda)$. The shading indicates a transition between active fluids ($D_L/D_S > 1$) and solids ($D_L/D_S < 1$). The inset depicts the normalized $D(t)$ for $\rho\lambda^2 = 0.01$ and $\tilde{q} \in \{0, 0.5, 0.6, 0.8\}$, demonstrating the transition from subdiffusive to ballistic intermediate behavior with increasing $\tilde{q}$. The dashed lines represent the analytical solutions of the Langevin equation for the diffusion of a doublet in the dilute limit, Eq. (11), the solid lines and symbols show numerical results.

$$\gamma \frac{\partial \mathbf{X}(t)}{\partial t} = \mathbf{A}(\tilde{q}) \cdot \mathbf{X}(t) + \mathbf{T}(t), \tag{10}$$

where $\mathbf{X}(t) = \{\delta r_A(t), \delta r_B(t)\}$ is the vector of the particle positions and $\mathbf{T}(t) = \{\xi_1(t), \xi_2(t)\}$ the vector with the random (radial) forces acting on the particles. For simplicity, we set the friction coefficient γ independent of the particle index. Using variation of constants, this differential equation is solved by the integration over a matrix exponential

$$\mathbf{X}(t) = \frac{1}{\gamma} \int_0^t \mathrm{d}\tau \ \exp\left[\mathbf{A}\,(t-\tau)/\gamma\right] \cdot \mathbf{T}(\tau),$$

with $\langle \mathbf{T}(t) \rangle = 0$ and $\langle \mathbf{T}_i(t) \cdot \mathbf{T}_j(t') \rangle = 2\gamma k_B T \delta_{ij} \delta(t-t')\mathbf{I}$, leading to $\langle \mathbf{X}(t) \rangle = 0$. By computing the mean squared displacement, we determine the diffusion ratio,

$$\frac{D_L(\tilde{q})}{D_S} = \frac{C_A^2(\tilde{q}) + C_B^2(\tilde{q})}{\left[C_A(\tilde{q}) + C_B(\tilde{q})\right]^2}. \tag{11}$$

The result of Eq. (11), the long-time diffusion coefficient D_L normalized by the short-time coefficient $D_S = \lim_{t\to 0} D(t) = k_B T/\gamma$, is presented in Figs. 8 and 9 by the black dashed line.

Finally, we demonstrate the impact of finite temperatures in many-body simulations. In Fig. 8, we compare the analytical results for the diffusion coefficient, Eq. (11), with the numerical results obtained for number density $\rho\lambda^2 = 0.01$. The time-dependent diffusion coefficient $D(t) = \frac{1}{4t}\langle |\mathbf{r}(t) - \mathbf{r}(0)|^2 \rangle$ plotted in Fig. 8 saturates towards D_L. For intermediate times there is either a sub-diffusive regime due to particle caging, or a ballistic regime arising from the emerging activity.[27,28] As discussed above (see Fig. 2), in dilute systems the activity at finite temperatures is expected to set in at $\tilde{q} > \tilde{q}_{\mathrm{cr1}} (\simeq 0.46)$. From Fig. 8 we see that for $\rho\lambda^2 = 0.01$ the transition to active fluids, $D_L/D_S > 1$, indeed occurs near this value. The long-time diffusion increases over several orders of magnitude as a function of nonreciprocity $\tilde{q}$. Even in dense colloidal fluids (at $\rho\lambda^2 = 1.75$) the ratio D_L/D_S exceeds 5, implying that there is an enormous diffusivity relative to the case of infinite dilution. As revealed by the snapshots in Fig. 5, this is mainly due to significant local alignment in

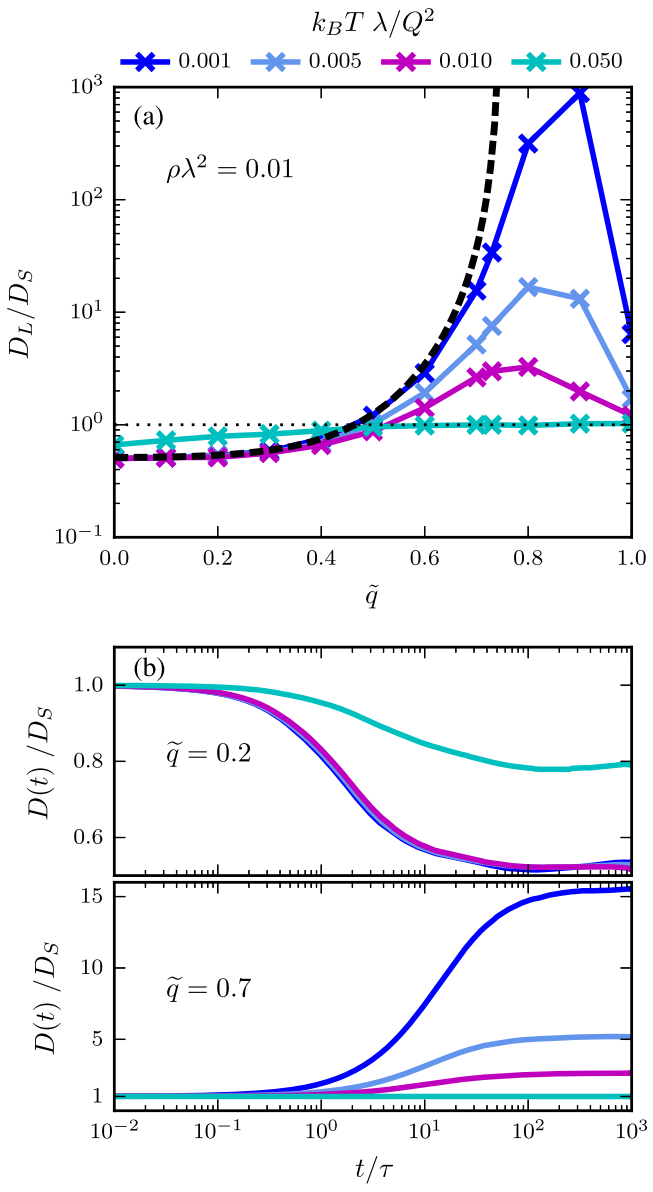

FIG. 9. (a) Ratio of the long-time to short-time diffusion coefficients, D_L/D_S, obtained from the time dependent diffusion coefficient $D(t)$ for given finite temperatures and number density $\rho\lambda^2 = 0.01$. The horizontal dotted line indicates the transition between active fluids ($D_L/D_S > 1$) and solids ($D_L/D_S < 1$). The dashed line represents the analytical solution, the solid lines and symbols show numerical results. (b) Temporal evolution of $D(t)$ normalized by D_S for two chosen relative wake charges $\tilde{q} = 0.2$ and $\tilde{q} = 0.7$ with $\rho\lambda^2 = 0.01$ and varied finite temperature.

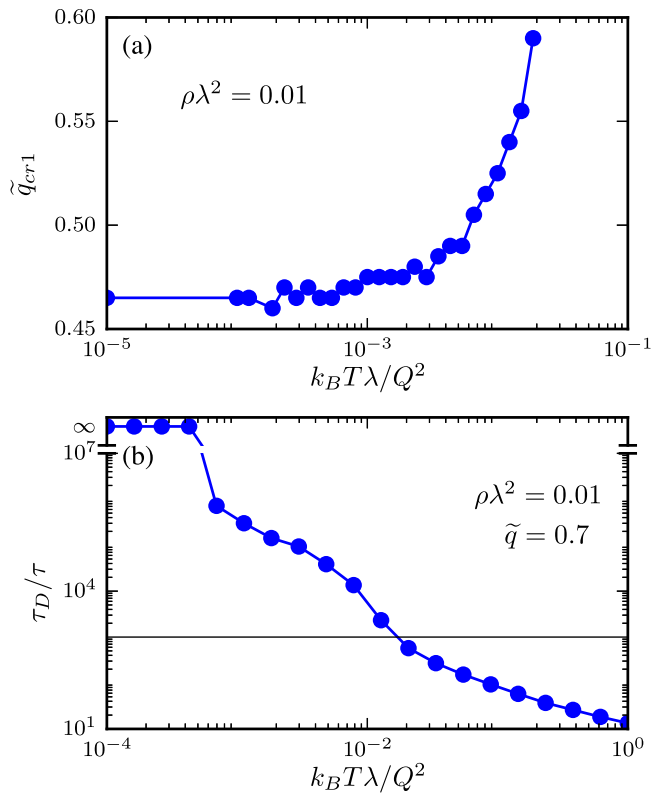

FIG. 10. (a) Temperature dependence of the onset of activity $\tilde{q}_{\mathrm{cr1}}$ (determined from the condition $D_L/D_S > 1$) in simulations with $\rho\lambda^2 = 0.01$. At low temperatures it approaches the analytically derived value of $\tilde{q}_{\mathrm{cr1}} \simeq 0.46$. (b) Temperature dependence of the doublet decay time τ_D for simulations with $\rho\lambda^2 = 0.01$ and $\tilde{q} = 0.7$. If no pair splits during the simulation time, τ_D is set to infinity. The horizontal line shows the stability criterion of long-living active clusters.

the fluid, which allows for an efficient traveling of active doublets.

One can see that the onset of activity, defined by the diffusion ratio $D_L/D_S > 1$, remains practically unchanged at all temperatures, whereas the asymptotic deviation of $D(t)/D_S$ from unity decreases with T, see Fig. 9. Naturally, at higher temperatures the stability is gradually decreasing. The explicit dependence of the activity onset ($\tilde{q}_{\mathrm{cr1}}$) and pair stability (τ_D) on the temperature is shown in Fig. 10.

VI. CONCLUSION

In conclusion, we have shown that in two-dimensional systems with wake-mediated interactions a rich variety of self-organization phenomena occur. In the zero-temperature limit, the nonreciprocal forces exerted by wakes generate a complex diagram of steady states. In particular, we showed the formation of active units — bound particle pairs, having interesting similarities with permanently active Brownian particles — and the realization of unusual melting scenarios. At finite temperatures we identified regimes of anomalously high diffusion. The ability of particles with the wake-mediated interactions to form active units, the unusual melting and the unique diffusive behavior make such systems interesting for many fields of research. We encourage scientists in the field of colloidal dispersions or complex plasmas to realize the experiments where these theoretical predictions can be verified.

ACKNOWLEDGMENTS

The authors acknowledge support from the European Research Council, under the European Union's Seventh Framework Programme, ERC Grant Agreement No. 267499, and from the Russian Scientific Foundation, Project No. 14-43-00053. A.K. gratefully acknowledges financial support through a Postdoctoral Research Fellowship (KA 4255/1-1) from the Deutsche Forschungsgemeinschaft (DFG).

[1]K. Hayashi and S. Sasa, J. Phys.: Condens. Matter **18**, 2825 (2006).
[2]P. Buenzli and R. Soto, Phys. Rev. E **78**, 020102 (2008).
[3]K. Dholakia and P. Zemánek, Rev. Mod. Phys. **82**, 1767 (2010).
[4]E. R. Shanblatt and D. G. Grier, Opt. Express **19**, 5833 (2011).
[5]B. Sabass and U. Seifert, Phys. Rev. Lett. **105**, 218103 (2010).
[6]R. Soto and R. Golestanian, Phys. Rev. Lett. **112**, 068301 (2014).
[7]A. V. Ivlev, H. Löwen, G. E. Morfill, and P. C. Royall, *Complex Plasmas and Colloidal Dispersions: Particle-resolved Studies of Classical Liquids and Solids* (World Scientific, 2012).
[8]M. Bonitz, C. Henning, and D. Block, Rep. Prog. Phys. **73**, 066501 (2010).
[9]G. E. Morfill and A. V. Ivlev, Rev. Mod. Phys. **81**, 1353 (2009).
[10]M. Chaudhuri, A. V. Ivlev, S. A. Khrapak, H. M. Thomas, and G. E. Morfill, Soft Matter **7**, 1287 (2011).
[11]A. Melzer, V. A. Schweigert, I. V. Schweigert, A. Homann, S. Peters, and A. Piel, Phys. Rev. E **54**, R46 (1996).
[12]A. V. Ivlev, J. Bartnick, M. Heinen, C.-R. Du, V. Nosenko, and H. Löwen, Phys. Rev. X **5**, 011035 (2015).
[13]A. S. Khair and J. F. Brady, Proc. R. Soc. A **463**, 223 (2007).
[14]C. Mejía-Monasterio and G. Oshanin, Soft Matter **7**, 993 (2011).
[15]J. Dzubiella, H. Löwen, and C. N. Likos, Phys. Rev. Lett. **91**, 248301 (2003).
[16]R. Soto and R. Golestanian, Phys. Rev. E **91**, 052304 (2015).
[17]I. Buttinoni, G. Volpe, F. Kümmel, G. Volpe, and C. Bechinger, J. Phys.: Condens. Matter **24**, 284129 (2012).
[18]M. E. Leunissen, C. G. Christova, A.-P. Hynninen, C. P. Royall, A. I. Campbell, A. Imhof, M. Dijkstra, R. van Roj, and A. van Blaaderen, Nature **437**, 235 (2005).
[19]P. Romanczuk, M. Bär, W. Ebeling, B. Linder, and L. Schimansky-Geier, Eur. Phys. J.: Spec. Top. **202**, 1 (2012).
[20]J. Elgeti, R. G. Winkler, and G. Gompper, Rep. Prog. Phys. **78**, 056601 (2015).
[21]M. Doi and S. Edwards, *The Theory of Polymer Dynamics* (Clarendon Press, 1986).
[22]A. Awazu, Phys. Rev. E **90**, 042308 (2014).
[23]N. Ganai, S. Sengupta, and G. I. Menon, Nucleic Acids Res. **42**, 4145 (2014).
[24]A. Bérut, A. Petrosyan, and S. Ciliberto, Europhys. Lett. **107**, 60004 (2014).
[25]A. Y. Grosberg and J.-F. Joanny, Phys. Rev. E **92**, 032118 (2015).
[26]S. N. Weber, C. A. Weber, and E. Frey, Phys. Rev. Lett. **116**, 058301 (2016).
[27]J. R. Howse, R. A. L. Jones, A. J. Ryan, T. Gough, R. Vafabakhsh, and R. Golestanian, Phys. Rev. Lett. **99**, 048102 (2007).
[28]X. Zheng, B. ten Hagen, A. Kaiser, M. Wu, H. Cui, Z. Silber-Li, and H. Löwen, Phys. Rev. E **88**, 032304 (2013).
[29]L. Baraban, D. Makarov, R. Streubel, I. Mönch, D. Grimm, S. Sanchez, and O. G. Schmidt, ACS Nano **6**, 3383 (2012).
[30]R. Grima, Phys. Rev. Lett. **95**, 128103 (2005).
[31]The wake potential in a plasma is characterized by a complicated (non-exponential) screening. However, the resulting deviations from the Yukawa model of the wake-mediated interactions were shown to have only a minor quantitative effect on the dynamics.[42,43]
[32]L. Couëdel, V. Nosenko, A. V. Ivlev, S. K. Zhdanov, H. M. Thomas, and G. E. Morfill, Phys. Rev. Lett. **104**, 195001 (2010).
[33]A. V. Ivlev and G. E. Morfill, Phys. Rev. E **63**, 016409 (2000).
[34]Given the vertical separation of particles within an active unit, we refrain from the term active molecules used in Ref. 6.
[35]See supplementary material at http://dx.doi.org/10.1063/1.4953225 for movies.
[36]P. H. Colberg and F. Höfling, Comput. Phys. Commun. **182**, 1120 (2011).
[37]A. M. Menzel and T. Ohta, Europhys. Lett. **99**, 58001 (2012).
[38]F. Alarcón and I. Pagonabarraga, J. Mol. Liq. **185**, 56 (2013).
[39]M. Hennes, K. Wolff, and H. Stark, Phys. Rev. Lett. **112**, 238104 (2014).
[40]Y. Fily and M. C. Marchetti, Phys. Rev. Lett. **108**, 235702 (2012).
[41]C. Reichhardt and C. J. O. Reichhardt, Phys. Rev. E **91**, 032313 (2015).
[42]T. B. Röcker, A. V. Ivlev, R. Kompaneets, and G. E. Morfill, Phys. Plasmas **19**, 033708 (2012).
[43]T. B. Röcker, S. K. Zhdanov, A. V. Ivlev, M. Lampe, G. Joyce, and G. E. Morfill, Phys. Plasmas **19**, 073708 (2012).